

ADT: Tuning Diffusion Models with Adversarial Supervision

Dazhong Shen¹ Guanglu Song¹ Yi Zhang¹ Bingqi Ma¹ Lujundong Li¹ Dongzhi Jiang¹ Zhuofan Zong¹
Yu Liu¹

Abstract

Diffusion models have achieved outstanding image generation by reversing a forward noising process to approximate true data distributions. During training, these models predict diffusion scores from noised versions of true samples in a single forward pass, while inference requires iterative denoising starting from white noise. This training-inference divergences hinder the alignment between inference and training data distributions, due to potential prediction biases and cumulative error accumulation. To address this problem, we propose an intuitive but effective fine-tuning framework, called Adversarial Diffusion Tuning (ADT), by stimulating the inference process during optimization and aligning the final outputs with training data by adversarial supervision. Specifically, to achieve robust adversarial training, ADT features a siamese-network discriminator with a fixed pre-trained backbone and lightweight trainable parameters, incorporates an image-to-image sampling strategy to smooth discriminative difficulties, and preserves the original diffusion loss to prevent discriminator hacking. In addition, we carefully constrain the backward-flowing path for back-propagating gradients along the inference path without incurring memory overload or gradient explosion. Finally, extensive experiments on Stable Diffusion models (v1.5, XL, and v3), demonstrate that ADT significantly improves both distribution alignment and image quality.

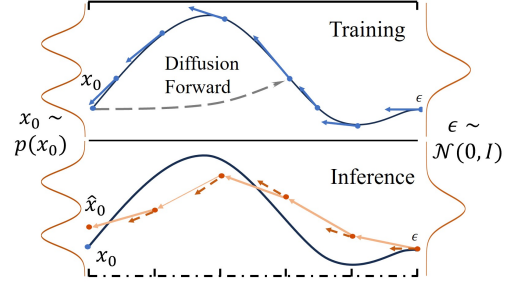


Figure 1. A simple illustration for the training-inference divergence. The training procedure aims to fit the score function $\nabla_x \log p(x, t)$ at every time step with access to real data, while the inference turns to denoise from white noise through a fixed path without the exact score estimation and real data.

noise ϵ_t as time grows, while the samples can be recovered by the reversed SDE with approximated score estimation $s_\theta \approx \nabla_x \log p(x, t)$ iteratively.

Unlike previous generative models such as Generative Adversarial Networks (GANs) (Goodfellow et al., 2020) and Variational Autoencoders (VAEs) (Kingma & Welling, 2013), which integrate the entire inference process into the optimization, diffusion models are prone to suffer from training-inference discrepancies (Ning et al., 2023b). Specifically, as shown in Fig. 1, during each training step, a time step t is first sampled randomly. The diffusion model then predicts the current score $\nabla_x \log p(x, t)$ based on the noised version x_t of the ground truth sample x_0 , requiring only a single forward pass. In contrast, during inference, samples are generated iteratively from white noise by denoising it through a fixed and sparse timestep sequence without access to the ground truth data. Each inference step is conducted based on the previously generated sample \hat{x}_t and not exact score estimation s_θ . In addition, conditional guidance strategies, such as classifier-free guidance (Ho & Salimans, 2022), may be employed in the text-to-image task, which is not available during training. As a result, the training optimization cannot fully access the inference procedure and generative distribution in practice, limiting the ability for distribution alignment.

To align the generative and real data distribution, researchers have made several efforts to alleviate those training-inference divergences from different views. For instance, some works focus on aligning the model input errors between training and inference. They propose to perturb the

1. Introduction

Diffusion models have recently been proven to be highly effective for image generation (Sohl-Dickstein et al., 2015; Ho et al., 2020) with outstanding quality and generalization (Podell et al., 2023; Esser et al., 2024). In particular, the key feature of diffusion models is to approximate the training data distribution $p(x)$ by a reversal of a continuous Stochastic Differential Equation (SDE). The forward SDE progressively corrupts images x with Gaussian

¹SenseTime.

training input (Ning et al., 2023b) to stimulate the input bias during inference and enhance the model robustness, or scale model output (Ning et al., 2023a) and shift timesteps (Li et al., 2023) to reduce sampling error accumulation along the inference path. Other researchers try to modify the diffusion sampler to align the practical inference path and the trajectory of the original reversed SDE, such as deriving the analytic forms for different sampling function parts (Bao et al., 2022), or applying different numerical solvers with varying accuracies and stability (Nichol & Dhariwal, 2021; Karras et al., 2022), such as DDIM (Song et al., 2020a) and DPMSlover (Lu et al., 2022a). However, given the various empirical inference tricks independent of the training process, such as using Classifier-free Guidance (Ho & Salimans, 2022) (CFG) or specifying inference timesteps, it is challenging to directly optimize the diverse errors and biases uniformly caused by training-inference divergences.

In this paper, we propose a unified fine-tuning framework called Adversarial Diffusion Tuning (ADT) to directly close the generative and training data distributions. Inspired by GANs and VAEs, our main idea is to simulate the inference process during optimization, allowing the final images to be affected by various practical errors, and using adversarial supervision to align them with training data. However, there exist two important challenges behind the optimization of ADT: 1) **(Adversarial Optimization.)** Adversarial models are well-known for their unstable training (Bai et al., 2021), which can be exacerbated with the large-scale diffusion models. To achieve robust optimization, we first propose a siamese-network-based discriminator with a frozen pre-trained image representation model as the backbone and a twin set of trainable lightweight discriminator heads, with the similarity-based discriminator score between the generative and real images. Additionally, instead of only inferring from the white noise, an image-to-image inference process, starting from a noisy image x_t at a random timestep t is incorporated for smoothing the adversarial distance between the generative and real data. Meanwhile, the original diffusion loss is preserved during optimization to prevent discriminator hacking. 2) **(Backward-Flowing Path.)** The introduction of the iterative inference paradigm significantly increases memory consumption and the risk of gradient explosion when back-propagating gradients along the reversed inference path. Here, we stop the gradients of the input for each iteration function except for one time of the input itself, allowing the model at each inference step to be updated efficiently and equally, even for the very early step. Finally, we validate the effectiveness of ADT on widely recognized text-to-image diffusion models with different model formulations, network architecture, and parameter scales, such as stable diffusion v1.5 (0.9B) (Rombach et al., 2022) and stable diffusion XL (3.5B) (Podell et al., 2023) and stable diffusion 3 (2B) (Esser et al., 2024). Extensive experimental

results show the advancements of ADT.

2. Preliminary

2.1. Diffusion Models

Given the image data space \mathcal{X} with an unknown distribution $p(x_0)$. Diffusion models (Sohl-Dickstein et al., 2015; Ho et al., 2020) define a forward process $\{x_t\}_{t \in [0, T]}$ for each image sample x_0 by a SDE equation:

$$dx_t = f(t)x_t dt + g(t)dw, \quad x_0 \sim p(x_0), \quad (1)$$

where w_t is the standard Wiener process, which indicates the image x_0 is corrupted by Gaussian noise as timestep t grows. Specifically, for any t , the variable x_t satisfies $x_t = \alpha_t x_0 + \sigma_t \epsilon$, $\epsilon \sim \mathcal{N}(0, I)$, where α_t and σ_t are smooth scalar function of t and referred as the noise schedule. In particular, when $t = T$, $x_T = \epsilon$. Under some regularity conditions, the reverse process of the above forward process has an associated probability flow ODE starting from time T , which has the same marginal distribution at time 0 as that of the backward SDE (Song et al., 2020b), i.e.,

$$dx_t = \left[f(t)x_t - \frac{g^2(t)}{2} \nabla_x \log q_t(x_t) \right] dt. \quad (2)$$

During learning, a neural network $\epsilon_\theta(x_t, t)$ would be used to estimate the scaled score function: $-\sigma_t \nabla_x \log q_t(x_t)$, which is also the predication of the used forward noise ϵ . Therefore, the optimization objective is $\mathbb{E}_{x_0, \epsilon, t} [\|\epsilon - \epsilon_\theta(x_t, t)\|_2^2]$. In practice, the inference process can be conducted by solving the ODE along a discrete timestep path $T = t_m > t_{m-1} > \dots > t_0 = 0$ with various ODE solvers, such as DDIM (Song et al., 2020a), DPMSlover (Lu et al., 2022a), etc. For all ODE solvers, each inference step can be represented with an abstracted sampler:

$$x_{t_{i-1}} = a_{t_i} x_{t_i} + b_{t_i} \epsilon_\theta(x_{t_i}, t_i), \quad (3)$$

where a_{t_i} and b_{t_i} can be determined by noise schedules and vary depending on the ODE solver used. In addition, for the text-to-image task, the Classifier-Free Guidance (CFG) (Ho & Salimans, 2022) strategy is widely used to follow the conditional prompt c with a conditional noise predictor $\epsilon_\theta(x_t, c, t)$. Specifically, CFG combines the unconditional/conditional models and obtains a new noise predictor: $\epsilon'_\theta(x_{t_i}, c, t_i) = (\gamma - 1)\epsilon_\theta(x_{t_i}, t_i) + \gamma\epsilon_\theta(x_{t_i}, c, t_i)$, where γ is the guidance scale that controls the image-prompt alignment. Note that, for simplicity, we only use the signals from unconditional sampling. This approach can be easily extended to scenarios involving the CFG strategy

2.2. Back-Propagation for Iterative Sampling

Optimizing diffusion models using gradients on the output image from iterative inference has become crucial for captur-

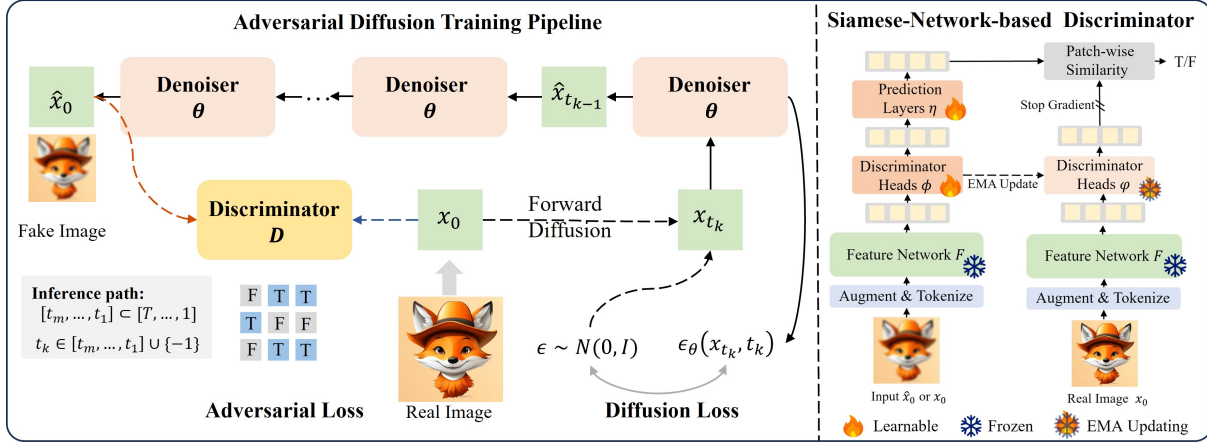


Figure 2. The overview framework of our ADT model.

ing properties that are challenging to address in a single diffusion step, such as human preference (Kirstain et al., 2023; Wu et al., 2023b) and aesthetic evaluation (Murray et al., 2012). However, a dilemma will arise: back-propagating gradients through the inference path to earlier steps incurs substantial computational overhead and risks gradient explosion (Clark et al., 2023). To mitigate these risks, some works (Clark et al., 2023; Xu et al., 2024a; Prabhudesai et al., 2023) constrain the back-propagation path to inference steps near the output image. Nevertheless, training only on the last few steps may be insufficient. More recently, DRTune (Wu et al., 2024) proposes blocking the gradient of the input for each noise estimation ϵ_θ , i.e.,

$$x_{t_{i-1}} = a_{t_i} x_{t_i} + b_{t_i} \epsilon_\theta(sg(x_{t_i}), t_i), \quad (4)$$

where $sg(\cdot)$ denotes the stop gradient operation, allowing the gradient to flow only through the term $a_{t_i} x_{t_i}$. In this manner, each inference step can be independently optimized, providing a stable way to control the backward gradient flow along the entire inference path. To further reduce memory, only a subset of inference steps can be sampled for training. Here, we further extend DRTune for the gradient back-propagation from the adversarial loss on the output image for stable and effective training.

3. Adversarial Diffusion Tuning

Our core idea is to incorporate the entire inference process into the model training process, where the inference images would be accessible for model optimization and are optimized in an adversarial manner. The left part of Figure 2 shows the overview training pipeline of ADT which involves two learnable networks: the pretrained diffusion model ϵ_θ with weights θ as the generator G_θ , and a discriminator D_ϕ with trainable weights ϕ . During training, the same sampling strategy π as that used during inference is applied to generate samples \hat{x}_0 and stimulate the generative image space $\mathcal{X}_{G_\theta}^\pi$. With true samples $x_0 \in \mathcal{X}$, the training

objective is to optimize the adversarial objective:

$$\min_{\theta} \max_{\phi} \mathcal{L}_{\text{adv}}(\mathcal{X}, \mathcal{X}_{G_\theta}^\pi; G_\theta, D_\phi, \pi) = \mathbb{E}_{x_0 \in \mathcal{X}} [\log(D_\phi(x_0))] + \mathbb{E}_{\hat{x}_0 \in \mathcal{X}_{G_\theta}^\pi} [\log(1 - D_\phi(\hat{x}_0))]. \quad (5)$$

Specifically, to ensure **training stability** during adversarial optimization, we enhance the overall procedure in three key aspects: reducing the number of learnable parameters in the discriminator, smoothing the adversarial distance through an image-to-image diffusion process, and incorporating the original diffusion loss to prevent knowledge forgetting. Additionally, for **efficient gradient back-propagation** through the inference path, we follow (Wu et al., 2023b) and use the stop gradient operation to constrain and deepen the backward-flowing path, allowing the model at each inference step to be updated equally without memory overload or gradient explosion. The overall training process can be found in Algorithm 1.

3.1. Adversarial Optimization

Siamese-Network based Discriminator. For the discriminator D , we follow (Sauer et al., 2023a) and use a frozen pre-trained feature network F with some trainable lightweight discriminator heads h_1, \dots, h_m . The right part of Figure 2 shows the overview network architecture. Specifically, We utilize DINOv2 (Oquab et al., 2023) as the feature network F , leveraging its state-of-the-art self-supervised visual representations learned from large-scale datasets. DINOv2 is implemented with a ViT backbone (Dosovitskiy et al., 2020). Each input image $x_I = \hat{x}_0$ or x_0 is first tokenized into a sequence of patches. We apply small convolutional discrimination heads h_i to the patch embeddings extracted from selected transformer blocks.

In particular, instead of directly outputting a scalar score by the discriminator head h_i , we introduce a dual network \hat{h}_i for each h_i with different weights φ . The discrimination

score is defined as the similarity between their output vectors z_I and z_R , corresponding to the input image x_I and the reference real image x_0 with the same prompt c , respectively. The idea behind this is inspired by the self-supervised learning approaches (Grill et al., 2020; Chen et al., 2020), where the generative image \hat{x}_0 is regarded as the augmented view of the corresponding reference image x_0 . The generator is optimized to generate similar images to reference images so that the corresponding output vectors z_I and z_R are close to each other. More specifically, we follow (Grill et al., 2020) and introduce a simple predictor network g_η on the vector z_I to predict the vector z_R . The discriminator score is defined as,

$$D_i(x_I) = \frac{\langle q_\eta(h_i(F(x_I))), h'_i(F(x_0)) \rangle}{\|q_\eta(h_i(F(x_I)))\|_2 \cdot \|h'_i(F(x_0))\|_2}. \quad (6)$$

where, the parameters φ in the dual head h'_i is without gradient backward and updated in each training step by the exponential moving average of the parameters ϕ of the corresponding head h_i , i.e., $\varphi \leftarrow \tau\varphi + (1 - \tau)\phi$ with the decay rate $\tau \in [0, 1]$.

Previous works report that two Siamese networks benefit from a robust optimization process (He et al., 2020; Grill et al., 2020), where we have also observed better performance in our practice. In particular, we apply differentiable data augmentation (Zhao et al., 2020) to the input image, \hat{x}_0 or x_0 , which has been proven to significantly improve performance (Sauer et al., 2023a).

Image-to-Image Inference. Actually, in the early training stages of ADT, there is a significant gap between the generative distribution and training data distribution, which can be recognized by the discriminator easily but is challenging for the generator to close. As a result, the training process would be unstable due to the optimization imbalance between the generator and discriminator. To address this problem, we further simulate the image-to-image inference process into the optimization.

Specifically, during each training iteration, the starting timestep t_s is first uniformly selected from the entire discrete inference path $\{T, t_{m-1}, \dots, 0\}$, and the initial latent image is defined as $x_{t_s} = \alpha_{t_s}x_0 + \sigma_{t_s}\epsilon$, where the noise ϵ is drawn from $\mathcal{N}(0, I)$. Intuitively, when t_s approaches 0, the initial image more closely resembles x_0 , resulting in an output image \hat{x}_0 that better aligns with the real sample x_0 . This provides a natural mechanism to reduce the divergence between generated outputs and training data. Formally, denoting $\mathcal{T}_{t_s \rightarrow 0}^\pi$ as the image-to-image inference path starting from timestep t_s along with the sampling strategy π . The adversarial loss in Equation 5 would be extended as:

$$\mathcal{L}_{\text{adv}} = \mathbb{E}_{t_s \sim \mathcal{U}(\pi)} [\mathcal{L}_{\text{adv}}(\mathcal{X}, \mathcal{X}_{G_\theta}; G_\theta, D_\phi, \mathcal{T}_{t_s \rightarrow 0}^\pi)]. \quad (7)$$

In particular, the CFG strategy is incorporated into each

Algorithm 1 The Training Procedure of ADM

```

1: Input: training set  $X$ , generator  $G_\theta$  with pre-trained
   model  $\epsilon_\theta$ , discriminator  $D$  with parameters  $\{\phi, \varphi, \eta\}$ ,
   sampling strategy  $\pi$  with the timestep set  $\{t_m, \dots, t_0\}$ ,
   learning rate  $\gamma$ , EMA rate  $\tau$ , hyper-parameters  $\lambda, H, K$ 
2: for iter = 1, 2, ...,  $N$  do
3:   Sample  $x_0 \in X, s \in [m, \dots, 0], \epsilon \sim \mathcal{N}(0, I)$ 
4:    $\hat{x}_0 = \alpha_{t_s}x_0 + \beta_{t_s}\epsilon, k = \min(K, s)$ 
5:   Sample  $\mathbb{S} = \{t_{k_j}\}_{j=1}^k \subset \{t_s, \dots, t_1\}$ 
6:   for  $t = t_s \dots, t_1$  do
7:     if  $t = t_s$  then
8:        $\bar{\epsilon} = \hat{\epsilon} = \epsilon_\theta(x, t)$ 
9:     else if  $t \in \mathbb{S}$  then
10:       $\hat{\epsilon} = \epsilon_\theta(sg(x), t)$ 
11:    else
12:       $\hat{\epsilon} = sg(\epsilon_\theta(x, t))$ 
13:    end if
14:     $\hat{x}_0 = \hat{x}_0 + (a_t - 1)sg(\hat{x}_0) + b_t\hat{\epsilon}$ 
15:  end for
16:  Compute  $\mathcal{L}_{\text{adv}}^D$  in Equ. 9 with  $x_0$  and  $\hat{x}_0$ 
17:  Update parameter  $[\phi, \eta] \leftarrow [\phi, \eta] - \beta \nabla_{\phi, \eta} \mathcal{L}_{\text{adv}}^D$ ,
18:  Update parameter  $\varphi \leftarrow \tau\varphi + (1 - \tau)\phi$ 
19:  if iter% $H = 0$  then
20:    Compute  $\mathcal{L}^G$  in Equ. 8 with  $\hat{x}_0, \bar{\epsilon}$  and  $\lambda$ 
21:    Update generator  $\theta \leftarrow \theta - \gamma \nabla_\theta \mathcal{L}^G$ 
22:  end if
23: end for
    
```

inference path $\mathcal{T}_{t_s \rightarrow 0}^\pi$ to align with practical inferences.

Joint Learning with Diffusion Loss. Note that, the optimizing direction of our adversarial loss may be largely different from that of the original diffusion loss, which may cause the problem of catastrophic forgetting, even the collapse of image quality. Therefore, we also preserve the original diffusion loss $\mathcal{L}_{\text{diff}}$ to guide the updating for the generator ϵ_θ . In addition, we use hinge loss (Lim & Ye, 2017) as the practical adversarial objective function. Then, the generator's objective amounts to:

$$\mathcal{L}^G = \mathbb{E}_{\substack{x_0 \in \mathcal{X} \\ t_s \sim \mathcal{U}(\pi) \\ \epsilon \sim \mathcal{N}(0, I)}} \left[- \sum_i D_i(\mathcal{T}_{t_s \rightarrow 0}^\pi(x_0, \epsilon; G_\theta)) + \lambda \|\epsilon_\theta(x_{t_s}, t_s) - \epsilon\|_2^2 \right], \quad (8)$$

where the first line represents the generator loss indicated as $\mathcal{L}_{\text{adv}}^G$ and the second line specifies the diffusion loss $\mathcal{L}_{\text{diff}}$, applied at the start timestep t_s of the inference path. λ is a hyper-parameter to balance the above two loss items. Correspondingly, the discriminator D is updated by minimizing the following objective,

$$\mathcal{L}_{\text{adv}}^D = \mathbb{E}_{\substack{x_0 \in \mathcal{X} \\ t_s \sim \mathcal{U}(\pi) \\ \epsilon \sim \mathcal{N}(0, I)}} \left[\sum_i \text{ReLU}(1 - D_i(x_0)) + \text{ReLU}(1 + D_i(\mathcal{T}_{t_s \rightarrow 0}^\pi(x_0, \epsilon; G_\theta))) \right], \quad (9)$$

In addition, to further balance the optimization of the generator and discriminator, we reduce the updating frequency of the generator to $1/H$, since the generator tends to easily hack the discriminator in our practice.

3.2. Backward-Flowing Path Constraint

At each training iteration for the diffusion model ϵ_θ , we need to back-propagate the gradient step-by-step from the final output image \hat{x}_0 to latent image x_{t_s} at the starting timestep t_s , where the memory consumption limit the depth of gradient back-propagation. A simple solution is DRTune (Wu et al., 2024), which applies the stop gradient operation on the model input during forward inference, as shown in Equ. 4. However, we argue that *DRTune suffers from rapid gradient explosion when backpropagating to the early inference timesteps*. Specifically, for the loss function \mathcal{L} on the final output \hat{x}_0 , the partial differential derivative on the latent image \hat{x}_{t_i} can be derived:

$$\frac{\partial \mathcal{L}(\hat{x}_0)}{\partial \hat{x}_{t_i}} = \frac{\partial \mathcal{L}(\hat{x}_0)}{\partial \hat{x}_0} \frac{\partial \hat{x}_0}{\partial \hat{x}_{t_i}} = \frac{\partial \mathcal{L}(\hat{x}_0)}{\partial \hat{x}_0} \prod_{j=1}^i a_{t_j}, \quad (10)$$

where a_{t_i} increases to a very large size when t_i grows to T with the common used linear or cosine noise scheduler (Chen, 2023) (See Appendix for more discussions). As a result, the gradient scale will explode rapidly for the early inference steps and lead to unstable optimization, where the scenario becomes worse in our adversarial training.

To balance the gradient scale on inference steps, we further propose to add the stop gradient operation on the linear part of the sampling equation, i.e.,

$$x_{t_{i-1}} = x_{t_i} + (a_{t_i} - 1)sg(x_{t_i}) + b_{t_i}\epsilon_\theta(sg(x_{t_i}), t_i), \quad (11)$$

Then, the backward gradient flows through the inference path without scale variation, i.e., $\partial L(\hat{x}_0)/\partial \hat{x}_{t_i} = \partial L(\hat{x}_0)/\partial \hat{x}_0$. Similar to DRTune (Wu et al., 2024), we select only K inference steps $\mathbb{S} = \{t_{k_j}\}_{j=1}^K$ for training; otherwise, the model ϵ_θ becomes detached from the backward-flowing path. The detailed forward inference process during training is presented at line 4-15 in Alg. 1. The corresponding updating gradient can be derived as:

$$\nabla_\theta \mathcal{L}^G = \frac{\partial \mathcal{L}_{adv}^G(\hat{x}_0)}{\partial \hat{x}_0} \sum_{t_i \in \mathbb{S}} b_{t_i} \frac{\partial \epsilon_\theta(\hat{x}_{t_i}, t_i)}{\partial \theta} + \lambda \frac{\partial \mathcal{L}_{diff}}{\partial \theta}. \quad (12)$$

3.3. Extension to Flow-Matching Model

In the above discussion, we take DDPM as the representative model. Actually, ADT can be easily extended to the flow-matching model (Liu et al., 2022; Esser et al., 2024), which is another state-of-the-art variant of diffusion models and has also been used widely (Esser et al., 2024; flu). Flow-matching models simplify the forward diffusion process as the linear interpolation of the real data and the white

noise $\epsilon \sim \mathcal{N}(0, I)$, i.e., $x_t = (1 - t)x_0 + t\epsilon$, $t \in [0, 1]$. A neural network $v_\theta(x_t, t)$ is optimized to estimate the conditional velocity $v(\epsilon) = \epsilon - x_0$ with the diffusion optimization loss $\mathcal{L}_{diff} = \mathbb{E}_{\epsilon, t, x_0} [\|v_\theta(x_t, t) - v(\epsilon)\|_2^2]$. With the same training pipeline as in Figure 2, the extension of ADT for flow-matching can be implemented by specifying the mechanism of the backward-flowing path constraint. Specifically, given the inference path $1 = t_m > \dots > t_0 = 0$, each inference step is conducted by:

$$x_{t_{k-1}} = x_{t_k} - (t_k - t_{k-1})v(sg(x_{t_k}), t_k). \quad (13)$$

4. Other Related Works and Comparisons

Technically, we stimulate the diffusion inference process during optimization and use adversarial supervision to close the generative and training distribution. In the literature, there exist some works that use similar technical parts.

Diffusion Optimization with Adversarial Objective.

Some recent works have tried to add the auxiliary adversarial loss between the final output and real data when optimizing the diffusion models (Sauer et al., 2023b). However, due to the potential gradient back-propagation problem, all of them predict the final output with only one or a few model forwards (Zhang et al., 2024; Ren et al., 2024). Meanwhile, to ensure the fidelity, the model forward should start near the end of the inference path (Ren et al., 2024), or the base model should be distilled to enhance the prediction accuracy for the early inference step, like ADD (Sauer et al., 2023b), UFOGen (Xu et al., 2024b). They all leverage an approximation of the practical generative distribution and lead to sub-optimal optimization results. In contrast, ADT introduces the whole inference procedure into the training process for stimulating the practical generative distribution. In particular, DMD2 (Yin et al., 2024) also stimulates the whole inference process during training. However, they focus on distilling diffusion models for accelerating sampling, where only 4 inference steps are considered during training. Here, we focus on improving the performance of the foundational diffusion models, which can also be further optimized or distilled for various downstream applications.

Diffusion Optimization with the Inference Procedure.

It is crucial to back-propagate through the iterative diffusion inference process when optimizing the assessment of the final generative images. Several works avoid the direct model parameters updating by optimizing the sampler parameters or input noise (Watson et al., 2022; Wallace et al., 2023). Other works use reinforcement learning to fine-tune model parameters without flowing gradients through the inference path (Black et al., 2023; Shen et al., 2023; Lee et al., 2023). Recently, researchers have also turned to constraining the backward-flowing path (Clark et al., 2023; Prabhudesai et al., 2023; Wu et al., 2024). However, they all rely on robust reward models on images or labor-intensive human

annotations to guide the optimization direction. Unlike previous methods, ADT can operate on the common image dataset without additional annotations. The discriminator acts as a reward model to assess image similarity to the training data, dynamically updating to reduce the risk of over-exploitation seen in previous approaches (Prabhudesai et al., 2023; Wu et al., 2024).

5. Experiments

Benchmark Models. We introduce two diffusion models and one flow-matching model as base models, which have different network backbones and parameter scales: 1) Stable Diffusion v 1.5 (**SD15**) (Rombach et al., 2022) is the typical text-to-image diffusion model, which applies the U-net (Ronneberger et al., 2015) with 0.86B parameters as the diffusion backbone; 2) Stable Diffusion XL base model (**SDXL**) (Podell et al., 2023) is the extended version of SD with overall 3.5B parameters. In particular, SDXL supports generating high-resolution images at 1024 resolution. 3) Stable Diffusion 3 medium (**SD3**) (Esser et al., 2024) is a large-scale flow matching model with transformers-based backbone, i.e., DiT (Peebles & Xie, 2023) with overall 2B parameters. SD15 can generate images of 512 resolution, while SDXL and SD3 support images at 1024 resolution.

Meanwhile, for SD15 and SDXL, two samplers are discussed, i.e., DDIM (Song et al., 2020a) with 50 diffusion steps, and DPMSlover++ (Lu et al., 2022b) (DPMS) with 30 diffusion steps, which are both the most widely used in practice. As for SD3, the original flow-matching sampler is used with 28 steps. The CFG strategy (Ho & Salimans, 2022) is also used for all three models with different guidance degrees, i.e., 7.0 for SD15 and SD3, and 5.0 for SDXL.

Dataset. To assess ADT’s ability to align generated and training data distributions, we increase optimization challenges by using training samples not included in the pre-training dataset. Along this line, we follow JourneyDB dataset (Sun et al., 2023) and collect 170K high-resolution and high-quality text-image pairs from Midjourney v6 (**mid**), a SOTA text-to-image generation online platform and released after the publication date of all three benchmark models. In particular, it commonly outputs high-quality images. Meanwhile, 10k text-image pairs are randomly selected for the test dataset if needed, while others are for training. Numerical statistics can be found in the Appendix.

Metric. We evaluate ADT with three types of metrics: 1) Firstly, following (Goodfellow et al., 2020; Rombach et al., 2022), we use the Frechet Inception Distance Score (**FID**) between the generative and the test datasets as the direct metric of the divergence of generative and training distributions. 2) Secondly, generated images ideally match the quality of the training data when their distributions align. With high-quality images as training data, the trained models should

also output high-quality images. We used two image quality assessment models for evaluation: HPSv2 Score (**HPS**) (Wu et al., 2023a), and Aesthetics Score (**AES**) (Schuhmann, 2022), which are trained to align the human preference with different network architectures. The HPSv2 benchmark prompts are used for the test, including 3200 captions with diverse styles. 3) Thirdly, **Human-level evaluation** is also involved in assessing whether quality truly improves after training on high-quality datasets

Training Settings. We use AdamW (Kingma, 2014) as the optimizer for both the discriminator and generator. The whole training batch size is set as 8 with 4 NVIDIA A100 GPUs. We train at fixed square resolutions, i.e., 512 for SD and 1024 for SDXL and SD3. The learning rate is set as the same for the discriminator and generator, $5e-6$ for SD and $1e-6$ for SDXL and SD3. The linear warmup is used with 1000 steps for the discriminator and 500 steps for the generator. The generator updating frequency is $1/5$. The EMA rate τ is set as 0.99. The weight parameter λ is set as 0.5. The hyper-parameter K is set as 3. Our code will be publicly accessible after acceptance.

5.1. Overall Performance

Table 1 shows the overall quantitative performance of our ADT framework, where the original fine-tuning strategy (FT) is used as the baseline. Both ADT and FT are trained with the same number of training iterations, i.e. 20k. The original base model is also involved for clear comparison. Our ADT framework is trained with the same sampler setting used for the inference. For more fairness comparisons, we also illustrate the win rate for different training frameworks in terms of HPS and AES scores in Figure 3.

We can find that ADT achieves the best performance among all settings, which demonstrates that ADT can both close the distribution distance between training and generated data, and align the image quality with the training data. Interestingly, ADT achieves large improvement in the small model, i.e., SD15, than in the models with large parameter scales, i.e., SDXL and SD3, even reaching similar FID scores between SD15 and SD3. This may demonstrate that ADT can inspire the model to realize greater parameter utilization efficiency. In addition, SDXL-based models achieve better FID scores, as their base model’s generated data more closely aligns with our dataset. In contrast, the style of generated data for SD3 is largely different from our dataset, where the outputs of SD3 are more like real photos while our dataset from Midjourney is like painting. As a result, the FT strategy may not narrow this distribution gap well and perform worse in terms of HPS scores, while ADT can make up for this setback and achieve better performance. In particular, we have checked that ADT captures 51% of the pair-wise win rate compared with the base model.

Table 1. The overall quantitative performance of the ADT framework.

	SD15+DDIM50			SD15+DPMS30			SDXL+DDIM50			SDXL+DPMS30			SD3		
	FID↓	HPS↑	AES↑	FID↓	HPS↑	AES↑	FID↓	HPS↑	AES↑	FID↓	HPS↑	AES↑	FID↓	HPS↑	AES↑
Base	24.20	27.41	5.422	25.67	26.86	5.384	16.16	27.66	5.911	16.82	27.71	6.013	23.32	28.24	5.820
FT	16.89	27.37	5.821	19.26	27.39	5.827	12.01	27.94	5.967	12.35	27.96	6.082	14.74	28.17	5.948
ADT	13.69	27.59	5.952	14.65	27.67	5.910	11.57	28.01	6.110	12.07	28.07	6.122	13.49	28.26	5.963

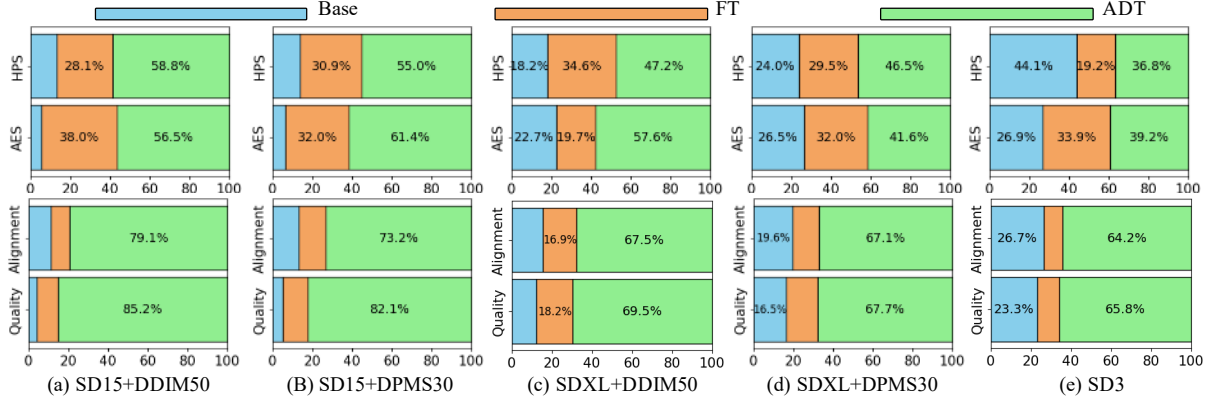


Figure 3. The win rate of different training strategies ranked by quality assessment models (Top) and human experts (Bottom).

Table 2. The performance of ADT when using an inference sampler different from the one used during training.

	DDIM Sampler			DPMS Sampler		
	FID-5k	HPS	AES	FID-5k	HPS	AES
FT	23.08	27.37	5.827	25.38	27.39	5.827
ADT-DDIM	19.84	27.60	5.952	20.73	27.67	5.925
ADT-DPMS	20.03	27.59	5.910	20.83	27.68	5.910

Figure 4 displays qualitative comparisons among different models with different training strategies. ADT produces more appealing imagery, with fine-grained details, vivid arrays of colors, and good composition. To be specific, images from FT and ADT models both present similar color and lighting styles to our dataset, while ADM models can also create more image details on animal hair, facial wrinkles, or object texture, and enrich the image background with reasonable color variations and object filling. Therefore, we further ask 5 experts to rank the generated images from models with different training strategies with 100 prompts randomly selected from HPS test prompts from two aspects: the image quality and text alignment. The results are summarized at the below line in Figure 3. ADT achieved an overwhelming victory on all three base models. More qualitative can be found in the Appendix.

5.2. Generalization for Samplers

Here, we further explore ADT’s generalization with different sampler settings. Specifically, we take the SD15 as an example and compare the performance of the trained model with different sampling settings or different samplers.

Different Sampling Settings. Using the DDIM sampler, we first fixed the inference steps as 50 and, vary the CFG

scales among [3.0, 5.0, 7.0, 9.0]. The assessment of generated images is shown in the top line of Figure 5. We can find our ADT framework can mostly achieve better performance compared with the original fine-tuning strategy with a lower FID score, and higher quality scores, i.e., HPS and AES scores. In addition, we can find that ADT can achieve a slower FID increase and faster HPS score increase when the CFG scale grows. Second, by fixing the CFG scale as 7.0, we vary the inference steps among [30, 50, 100, 200] and show the results in the bottom line of Figure 5. Our ADT framework has achieved a large performance improvement compared with FT in all settings with similar trends of change, where the performance will converge with 100 inference steps or more steps. All observations demonstrate the generalization of our ADT on varying sampling settings.

Different Sampling Methods. We further verify the generalization by using inconsistent inference samplers from those used during training. Table 2 presents the results. We observe that consistent inference samplers enable models to achieve the best scores across several metrics. For instance, ADT-DDIM with the DDIM sampler attains the best FID and AES scores, while ADT-DPMS with the DPMS sampler achieves the highest HPS score. Additionally, inconsistent samplers can yield similar results. The image quality may be less sensitive to the samplers used during training than the inference samplers.

5.3. Ablation Analysis

Here, we conduct the ablation analysis with three variants of our ADT framework: 1) + **StyleGAN** replace our discriminator with the discriminator used in StyleGAN-T (Sauer et al., 2023a), which also applies the pre-trained

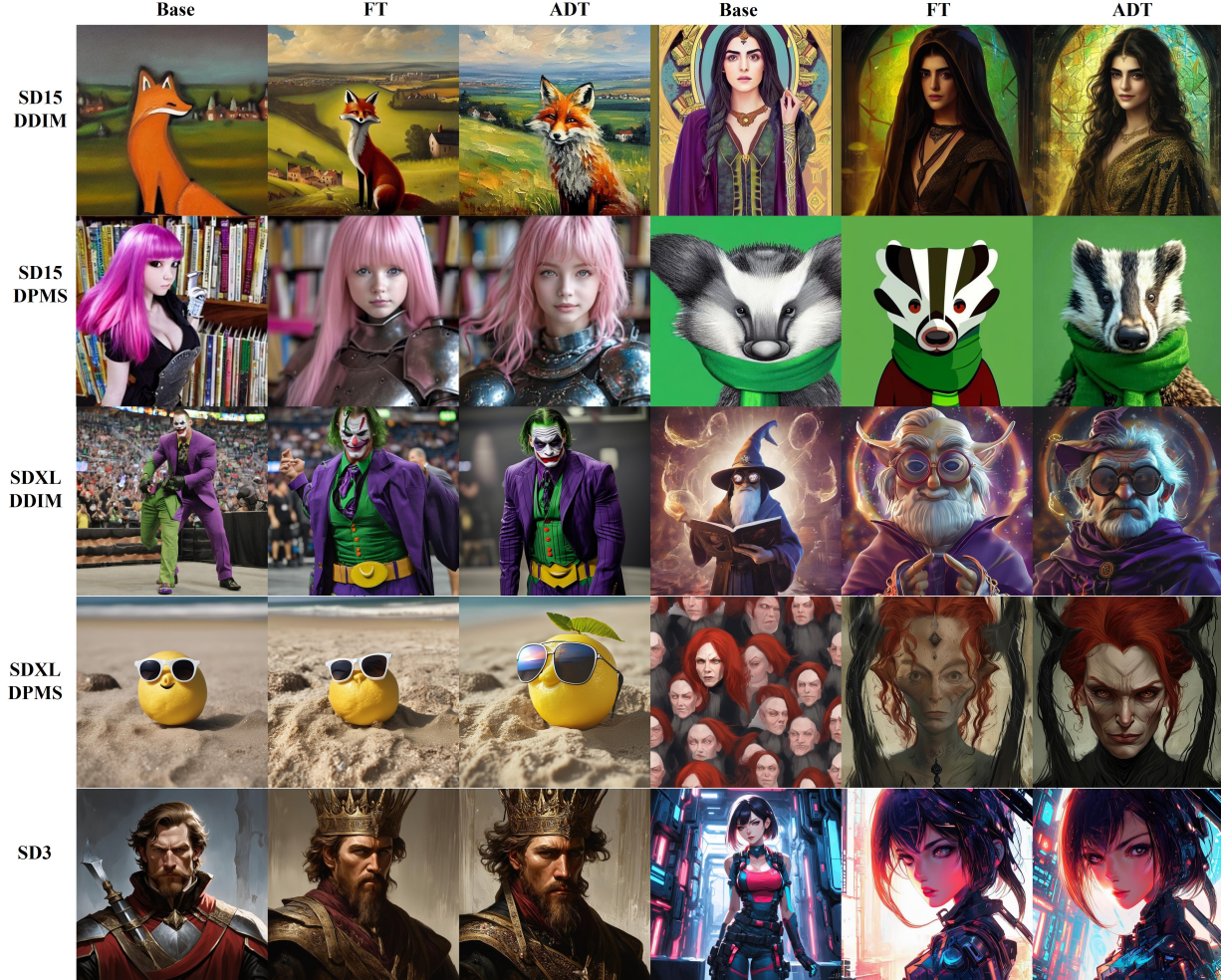


Figure 4. The generated samples under different training strategies, where captions sampled from HPSV2 Benchmark prompts.

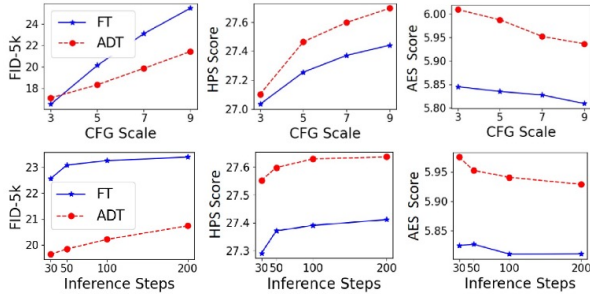


Figure 5. The performance of ADT with different CFG scales (Top) or numbers of inference steps (Bottom).

DINOv2 (Oquab et al., 2023) as the backbone without the siamese-network-based discriminator heads. 2) **+ DR-Tune** conduct the gradient backpropagation following DRTune (Wu et al., 2024) when the generator updating. 3) **w/o \mathcal{L}_{diff}** removes the original diffusion loss during training.

Take the SD15 as the example, we summarize the results in Table 3. We can find that our ADT has achieved the best performance with a large score margin compared with all

Table 3. The ablation analysis.

	FID-5k	HPS Score		AES Score	
		Score	Win Rate	Score	Win Rate
ADT	19.84	27.59	N/A	5.952	N/A
+ StyleGAN	22.35	27.48	0.5587	5.838	0.6381
+ DRTune	21.92	27.40	0.6014	5.849	0.6594
w/o \mathcal{L}_{diff}	24.03	27.18	0.7778	5.873	0.5993

variants. To be specific, removing the original diffusion loss significantly impairs the performance of distribution matching a lot, where the discriminator may be hacked. In addition, our siamese-network-based discriminator demonstrates superior performance compared to StyleGAN-based variants, while our constraints on the backward-flowing path are more effective than DRTune.

6. Conclusions

We propose Adversarial Diffusion Tuning (ADT), a fine-tuning framework that addresses training-inference divergence in diffusion models. The core idea is incorporating

the inference process into optimization and using adversarial objectives to align generative with training data. For robust adversarial supervision, ADT employs a siamese-network discriminator with a pre-trained backbone, utilizes an image-to-image sampling strategy, and preserves the original diffusion loss. We develop a backward-flowing path constraint mechanism to prevent memory overload and gradient explosion. Experiments across various diffusion models demonstrate ADT’s effectiveness.

7. Impact Statement

This paper presents work whose goal is to advance the field of Computer Vision and Machine Learning. There are many potential societal consequences of our work, none of which we feel must be specifically highlighted.

References

- Flux.1-dev. <https://huggingface.co/black-forest-labs/FLUX.1-dev>. Accessed: 2024 - 11- 14.
- Midjourney. <https://www.midjourney.com/home>. Accessed: 2024 - 11- 14.
- Bai, T., Luo, J., Zhao, J., Wen, B., and Wang, Q. Recent advances in adversarial training for adversarial robustness. *arXiv preprint arXiv:2102.01356*, 2021.
- Bao, F., Li, C., Zhu, J., and Zhang, B. Analytic-dpm: an analytic estimate of the optimal reverse variance in diffusion probabilistic models. *arXiv preprint arXiv:2201.06503*, 2022.
- Black, K., Janner, M., Du, Y., Kostrikov, I., and Levine, S. Training diffusion models with reinforcement learning. *arXiv preprint arXiv:2305.13301*, 2023.
- Chen, T. On the importance of noise scheduling for diffusion models. *arXiv preprint arXiv:2301.10972*, 2023.
- Chen, T., Kornblith, S., Norouzi, M., and Hinton, G. A simple framework for contrastive learning of visual representations. In *International conference on machine learning*, pp. 1597–1607. PMLR, 2020.
- Clark, K., Vicol, P., Swersky, K., and Fleet, D. J. Directly fine-tuning diffusion models on differentiable rewards. *arXiv preprint arXiv:2309.17400*, 2023.
- Dosovitskiy, A., Beyer, L., Kolesnikov, A., Weissenborn, D., Zhai, X., Unterthiner, T., Dehghani, M., Minderer, M., Heigold, G., Gelly, S., et al. An image is worth 16x16 words: Transformers for image recognition at scale. *arXiv preprint arXiv:2010.11929*, 2020.
- Esser, P., Kulal, S., Blattmann, A., Entezari, R., Müller, J., Saini, H., Levi, Y., Lorenz, D., Sauer, A., Boesel, F., et al. Scaling rectified flow transformers for high-resolution image synthesis. In *Forty-first International Conference on Machine Learning*, 2024.
- Goodfellow, I., Pouget-Abadie, J., Mirza, M., Xu, B., Warde-Farley, D., Ozair, S., Courville, A., and Bengio, Y. Generative adversarial networks. *Communications of the ACM*, 63(11):139–144, 2020.
- Grill, J.-B., Strub, F., Altché, F., Tallec, C., Richemond, P., Buchatskaya, E., Doersch, C., Avila Pires, B., Guo, Z., Gheshlaghi Azar, M., et al. Bootstrap your own latent-a new approach to self-supervised learning. *Advances in neural information processing systems*, 33:21271–21284, 2020.
- He, K., Fan, H., Wu, Y., Xie, S., and Girshick, R. Momentum contrast for unsupervised visual representation learning. In *Proceedings of the IEEE/CVF conference on computer vision and pattern recognition*, pp. 9729–9738, 2020.
- Ho, J. and Salimans, T. Classifier-free diffusion guidance. *arXiv preprint arXiv:2207.12598*, 2022.
- Ho, J., Jain, A., and Abbeel, P. Denoising diffusion probabilistic models. *Advances in neural information processing systems*, 33:6840–6851, 2020.
- Karras, T., Aittala, M., Aila, T., and Laine, S. Elucidating the design space of diffusion-based generative models. *Advances in neural information processing systems*, 35: 26565–26577, 2022.
- Kingma, D. P. Adam: A method for stochastic optimization. *arXiv preprint arXiv:1412.6980*, 2014.
- Kingma, D. P. and Welling, M. Auto-encoding variational bayes. *arXiv preprint arXiv:1312.6114*, 2013.
- Kirstain, Y., Polyak, A., Singer, U., Matiana, S., Penna, J., and Levy, O. Pick-a-pic: An open dataset of user preferences for text-to-image generation. *Advances in Neural Information Processing Systems*, 36:36652–36663, 2023.
- Lee, K., Liu, H., Ryu, M., Watkins, O., Du, Y., Boutilier, C., Abbeel, P., Ghavamzadeh, M., and Gu, S. S. Aligning text-to-image models using human feedback. *arXiv preprint arXiv:2302.12192*, 2023.
- Li, M., Qu, T., Yao, R., Sun, W., and Moens, M.-F. Alleviating exposure bias in diffusion models through sampling with shifted time steps. In *The Twelfth International Conference on Learning Representations*, 2023.
- Lim, J. H. and Ye, J. C. Geometric gan. *arXiv preprint arXiv:1705.02894*, 2017.

- Liu, X., Gong, C., and Liu, Q. Flow straight and fast: Learning to generate and transfer data with rectified flow. *arXiv preprint arXiv:2209.03003*, 2022.
- Lu, C., Zhou, Y., Bao, F., Chen, J., Li, C., and Zhu, J. Dpm-solver: A fast ode solver for diffusion probabilistic model sampling in around 10 steps. *Advances in Neural Information Processing Systems*, 35:5775–5787, 2022a.
- Lu, C., Zhou, Y., Bao, F., Chen, J., Li, C., and Zhu, J. Dpm-solver++: Fast solver for guided sampling of diffusion probabilistic models. *arXiv preprint arXiv:2211.01095*, 2022b.
- Murray, N., Marchesotti, L., and Perronnin, F. Ava: A large-scale database for aesthetic visual analysis. In *2012 IEEE conference on computer vision and pattern recognition*, pp. 2408–2415. IEEE, 2012.
- Nichol, A. Q. and Dhariwal, P. Improved denoising diffusion probabilistic models. In *International conference on machine learning*, pp. 8162–8171. PMLR, 2021.
- Ning, M., Li, M., Su, J., Salah, A. A., and Ertugrul, I. O. Elucidating the exposure bias in diffusion models. In *The Twelfth International Conference on Learning Representations*, 2023a.
- Ning, M., Sangineto, E., Porrello, A., Calderara, S., and Cucchiara, R. Input perturbation reduces exposure bias in diffusion models. In *International Conference on Machine Learning*, pp. 26245–26265. PMLR, 2023b.
- Oquab, M., Darcet, T., Moutakanni, T., Vo, H., Szafraniec, M., Khalidov, V., Fernandez, P., Haziza, D., Massa, F., El Nouby, A., et al. Dinov2: Learning robust visual features without supervision. *arXiv preprint arXiv:2304.07193*, 2023.
- Peebles, W. and Xie, S. Scalable diffusion models with transformers. In *Proceedings of the IEEE/CVF International Conference on Computer Vision*, pp. 4195–4205, 2023.
- Podell, D., English, Z., Lacey, K., Blattmann, A., Dockhorn, T., Müller, J., Penna, J., and Rombach, R. Sdxl: Improving latent diffusion models for high-resolution image synthesis. *arXiv preprint arXiv:2307.01952*, 2023.
- Prabhudesai, M., Goyal, A., Pathak, D., and Fragkiadaki, K. Aligning text-to-image diffusion models with reward backpropagation. *arXiv preprint arXiv:2310.03739*, 2023.
- Ren, Y., Wu, J., Lu, Y., Kuang, H., Xia, X., Wang, X., Wang, Q., Zhu, Y., Xie, P., Wang, S., et al. Byteedit: Boost, comply and accelerate generative image editing. *arXiv preprint arXiv:2404.04860*, 2024.
- Rombach, R., Blattmann, A., Lorenz, D., Esser, P., and Ommer, B. High-resolution image synthesis with latent diffusion models. In *Proceedings of the IEEE/CVF conference on computer vision and pattern recognition*, pp. 10684–10695, 2022.
- Ronneberger, O., Fischer, P., and Brox, T. U-net: Convolutional networks for biomedical image segmentation. In *Medical image computing and computer-assisted intervention–MICCAI 2015: 18th international conference, Munich, Germany, October 5–9, 2015, proceedings, part III 18*, pp. 234–241. Springer, 2015.
- Sauer, A., Karras, T., Laine, S., Geiger, A., and Aila, T. Stylegan-t: Unlocking the power of gans for fast large-scale text-to-image synthesis. In *International conference on machine learning*, pp. 30105–30118. PMLR, 2023a.
- Sauer, A., Lorenz, D., Blattmann, A., and Rombach, R. Adversarial diffusion distillation. *arXiv preprint arXiv:2311.17042*, 2023b.
- Schuhmann, C. Laion-aesthetics. <https://laion.ai/blog/laion-aesthetics/>, 2022. Accessed: 2023-11-10.
- Shen, X., Du, C., Pang, T., Lin, M., Wong, Y., and Kankanhalli, M. Finetuning text-to-image diffusion models for fairness. *arXiv preprint arXiv:2311.07604*, 2023.
- Sohl-Dickstein, J., Weiss, E., Maheswaranathan, N., and Ganguli, S. Deep unsupervised learning using nonequilibrium thermodynamics. In *International conference on machine learning*, pp. 2256–2265. PMLR, 2015.
- Song, J., Meng, C., and Ermon, S. Denoising diffusion implicit models. *arXiv preprint arXiv:2010.02502*, 2020a.
- Song, Y., Sohl-Dickstein, J., Kingma, D. P., Kumar, A., Ermon, S., and Poole, B. Score-based generative modeling through stochastic differential equations. *arXiv preprint arXiv:2011.13456*, 2020b.
- Sun, K., Pan, J., Ge, Y., Li, H., Duan, H., Wu, X., Zhang, R., Zhou, A., Qin, Z., Wang, Y., et al. Journeydb: A benchmark for generative image understanding. *Advances in Neural Information Processing Systems*, 36, 2023.
- Wallace, B., Gokul, A., Ermon, S., and Naik, N. End-to-end diffusion latent optimization improves classifier guidance. In *Proceedings of the IEEE/CVF International Conference on Computer Vision*, pp. 7280–7290, 2023.
- Watson, D., Chan, W., Ho, J., and Norouzi, M. Learning fast samplers for diffusion models by differentiating through sample quality. In *International Conference on Learning Representations*, 2022.

- Wu, X., Hao, Y., Sun, K., Chen, Y., Zhu, F., Zhao, R., and Li, H. Human preference score v2: A solid benchmark for evaluating human preferences of text-to-image synthesis. *arXiv preprint arXiv:2306.09341*, 2023a.
- Wu, X., Sun, K., Zhu, F., Zhao, R., and Li, H. Human preference score: Better aligning text-to-image models with human preference. In *Proceedings of the IEEE/CVF International Conference on Computer Vision*, pp. 2096–2105, 2023b.
- Wu, X., Hao, Y., Zhang, M., Sun, K., Huang, Z., Song, G., Liu, Y., and Li, H. Deep reward supervisions for tuning text-to-image diffusion models. *arXiv preprint arXiv:2405.00760*, 2024.
- Xu, J., Liu, X., Wu, Y., Tong, Y., Li, Q., Ding, M., Tang, J., and Dong, Y. Imagereward: Learning and evaluating human preferences for text-to-image generation. *Advances in Neural Information Processing Systems*, 36, 2024a.
- Xu, Y., Zhao, Y., Xiao, Z., and Hou, T. Ufogen: You forward once large scale text-to-image generation via diffusion gans. In *Proceedings of the IEEE/CVF Conference on Computer Vision and Pattern Recognition*, pp. 8196–8206, 2024b.
- Yin, T., Gharbi, M., Park, T., Zhang, R., Shechtman, E., Durand, F., and Freeman, W. T. Improved distribution matching distillation for fast image synthesis. *arXiv preprint arXiv:2405.14867*, 2024.
- Zhang, J., Wu, J., Ren, Y., Xia, X., Kuang, H., Xie, P., Li, J., Xiao, X., Huang, W., Zheng, M., et al. Unifl: Improve stable diffusion via unified feedback learning. *arXiv preprint arXiv:2404.05595*, 2024.
- Zhao, S., Liu, Z., Lin, J., Zhu, J.-Y., and Han, S. Differentiable augmentation for data-efficient gan training. *Advances in neural information processing systems*, 33: 7559–7570, 2020.
- .

A. Appendix

A.1. Gradient Explosion in DRTune (Wu et al., 2024)

When using DRTune (Wu et al., 2024) strategy for gradient back-propagation along with the reverse inference path, we can derive the partial differential derivative of the loss function \mathcal{L} on the latent image \hat{x}_{t_i} as the Equation 10, i.e.,

$$\frac{\partial \mathcal{L}(\hat{x}_0)}{\partial \hat{x}_{t_i}} = \frac{\partial \mathcal{L}(\hat{x}_0)}{\partial \hat{x}_0} \frac{\partial \hat{x}_0}{\partial \hat{x}_{t_i}} = \frac{\partial \mathcal{L}(\hat{x}_0)}{\partial \hat{x}_0} \prod_{j=1}^i a_{t_j}, \quad (\text{A1})$$

where a_{t_i} can be specified by the noise scheduler $\{\alpha_{t_i}, \sigma_{t_i}\}_i$ used in the forward diffusion process as the samplers used the inference process. Specifically, when using DDIM sampler (Ho et al., 2020) during inference, we can specify Equation 3 as,

$$x_{t_{i-1}} = \frac{\alpha_{t_{i-1}}}{\alpha_{t_i}} x_{t_i} + \left(\sqrt{1 - \alpha_{t_{i-1}}^2} - \frac{\alpha_{t_{i-1}} \sqrt{1 - \alpha_{t_i}}}{\alpha_{t_i}} \right) \epsilon(x_{t_i}, t_i). \quad (\text{A2})$$

Then, we can derive $\prod_{j=0}^i a_{t_j}$ as,

$$\prod_{j=0}^i a_{t_j} = \prod_{j=0}^i \frac{\alpha_{t_{j-1}}}{\alpha_{t_j}} = \frac{1}{\alpha_{t_i}}, \quad (\text{A3})$$

where α_{t_i} decreases to 0 as t_i increases T . Although α_T would not be set as 0 in practice, $\prod_{j=0}^i a_{t_j}$ would also increase rapidly as i grows. Figure A1 (a) shows the varying curve with 50 inference steps and linear or cosine noise scheduler, commonly used in practice. We also observe a very similar phenomenon for DPMSlover++ (Lu et al., 2022b) samplers as shown in Figure A1 (b), where the number of inference steps is 30.

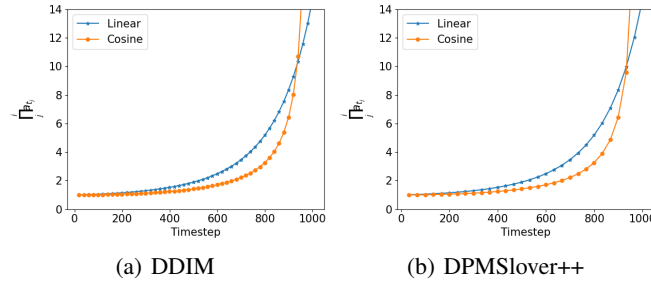


Figure A1. The curve of gradient scale $\prod_{j=1}^i a_{t_j}$ with different samplers.

A.2. Network Architecture for the Discriminator

The right part of Figure 2 shows the overview of the network architecture for our siamese-network-based discriminator. Here, we provide more details. Following StyleGAN2 (Sauer et al., 2023a), we apply the ViT-S network used in DINOv2 (Oquab et al., 2023) as the feature network F , where five transformer layers equally spaced with the layer numbers [2,5,8,11] are connected to the discriminator heads. The differentiable data augmentation (Zhao et al., 2020), including the translation padding, the Cutout square, and the color artifacts with the default, are applied on both the input image and the reference real image with the default settings in (Zhao et al., 2020). As for the discriminator heads, we use the same settings as that in StyleGAN-T (Sauer et al., 2023a), which consists of convolutions and batch normalization with the output channel as 64. The prediction layer η uses a similar network architecture to the discriminator heads with the input as 64.

A.3. Detailed Statistics of the Dataset

In our experiments, to assess ADT’s ability to align generated and training data distributions, we collect 170k high-resolution (1K) and high-quality text-image pairs from Midjourney v6 (mid), which have not been used during the pre-training of the benchmark models, i.e., Stable Diffusion v 1.5 (Rombach et al., 2022), Stable Diffusion XL (Podell et al., 2023), and Stable Diffusion 3 medium (Esser et al., 2024). The detailed numerical statistics can be found in Table A1.

A.4. Efficiency Analysis

In our ADT framework, we simulate the diffusion inference process during optimization and use adversarial supervision on the image space. Intuitively, ADT requires more computing cost compared with the original fine-tuning strategy, where

Table A1. The numerical statistics of our dataset.

	Instances	Tokens	HPS Score	AES Score
Training	160k	49.30	28.92	6.634
Test	10k	49.45	28.93	6.630

only one model forward is involved during each training step. However, we claim that ADT can outperform the FT strategy with less training steps. Taking SD15 as the example in Figure A2, ADT with 6k training steps has demonstrated better performance compared to the convergence achieved by FT.

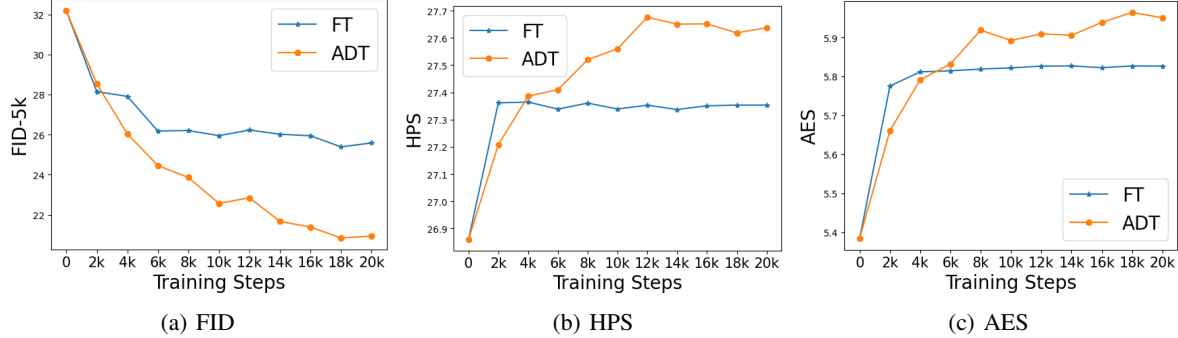


Figure A2. The performance curve during the optimization for SD15.

A.5. Experimental Results for the Text Alignment

In our experiments, we have evaluated the performance of ADT with three types of metrics: 1) FID, which measures the divergence of generative distribution and training data distributions. 2) Quality Assessment Model, i.e., HPSv2 Score (HPS) (Wu et al., 2023a) and Aesthetics Score (AES) (Schuhmann, 2022), which assess the image quality with the assessment models trained on the human preference feedback data. 3) Human-level evaluation of the image quality and text alignment. Here, we further verify the text alignment of the models trained by the ADT framework with the CLIP Score as the metric. Specifically, 5k prompts are randomly selected from our test data for generating images. Table A2 shows the results with different settings. We can find that our ADT framework can also increase the capability of text alignment in terms of the CLIP score. However, we claim that the CLIP score may not be a good metric when the prompt is too long.

Table A2. The evaluation of the text alignment with the CLIP score.

	Base	FT	ADT
SD15+DDIM50	0.3324	0.3339	0.3346
SD15+DPMS30	0.3313	0.3330	0.3340
SDXL+DDIM50	0.3677	0.3708	0.3759
SDXL+DPMS30	0.3712	0.3749	0.3758
SD3	0.3547	0.3616	0.3641

A.6. How to Choose λ

The hyper-parameter λ in Equation 8 aims to balance the adversarial loss and the original diffusion loss. The ablation analysis in Section 5.3 has demonstrated that the original diffusion loss is critical to avoiding knowledge forgetting and discriminator hacking. Here, we further conduct the sensitive analysis for λ . Taking SD15 as an example, where the DDIM sampler is used with 50 inference steps, we vary the λ among [0.1, 0.3, 0.5, 0.7, 1.0] and summarize the performances in Table A3. We can find that our ADT framework outperforms FT with $\lambda > 0$ on all three metrics, which demonstrates the superiority and robustness of ADT. In addition, ADT achieves the best scores in FID-5k and AES score when $\lambda = 0.5$, which is used in most of our experiments.

Table A3. The sensitive analysis of the hyper-parameter λ .

	FID-5k	HPS Score	AES Score
FT	23.08	27.37	5.821
$\lambda = 0.0$	24.07	27.18	5.873
$\lambda = 0.1$	21.11	27.53	5.924
$\lambda = 0.3$	20.35	27.64	5.938
$\lambda = 0.5$	19.84	27.59	5.952
$\lambda = 0.7$	20.03	27.65	5.924
$\lambda = 1.0$	19.93	27.66	5.917

A.7. More discussion about the Feature Network

In our experiments, the small version of DINOv2 is used for the backbone of the discriminator with 21M parameters. Here we further verify the performance of ADT with a larger feature network F , i.e., the large version of DINOv2 with 300M parameters, where five transformer layers with the layer numbers [5, 10, 14, 19, 23] are connected to the discriminator heads. Table A4 shows the results of the SD15 model with DDIM samplers and 50 inference steps. Interestingly, the larger pre-trained feature network, which is equipped with more powerful expression ability, has not brought significant improvement in our experiments, which needs more discussion in the future.

Table A4. The performance with large feature network.

	FID	HPS Score	AES Score
DINO-Small (21M)	19.84	27.59	5.952
ADT with DINO-Large (300M)	20.27	27.61	5.920

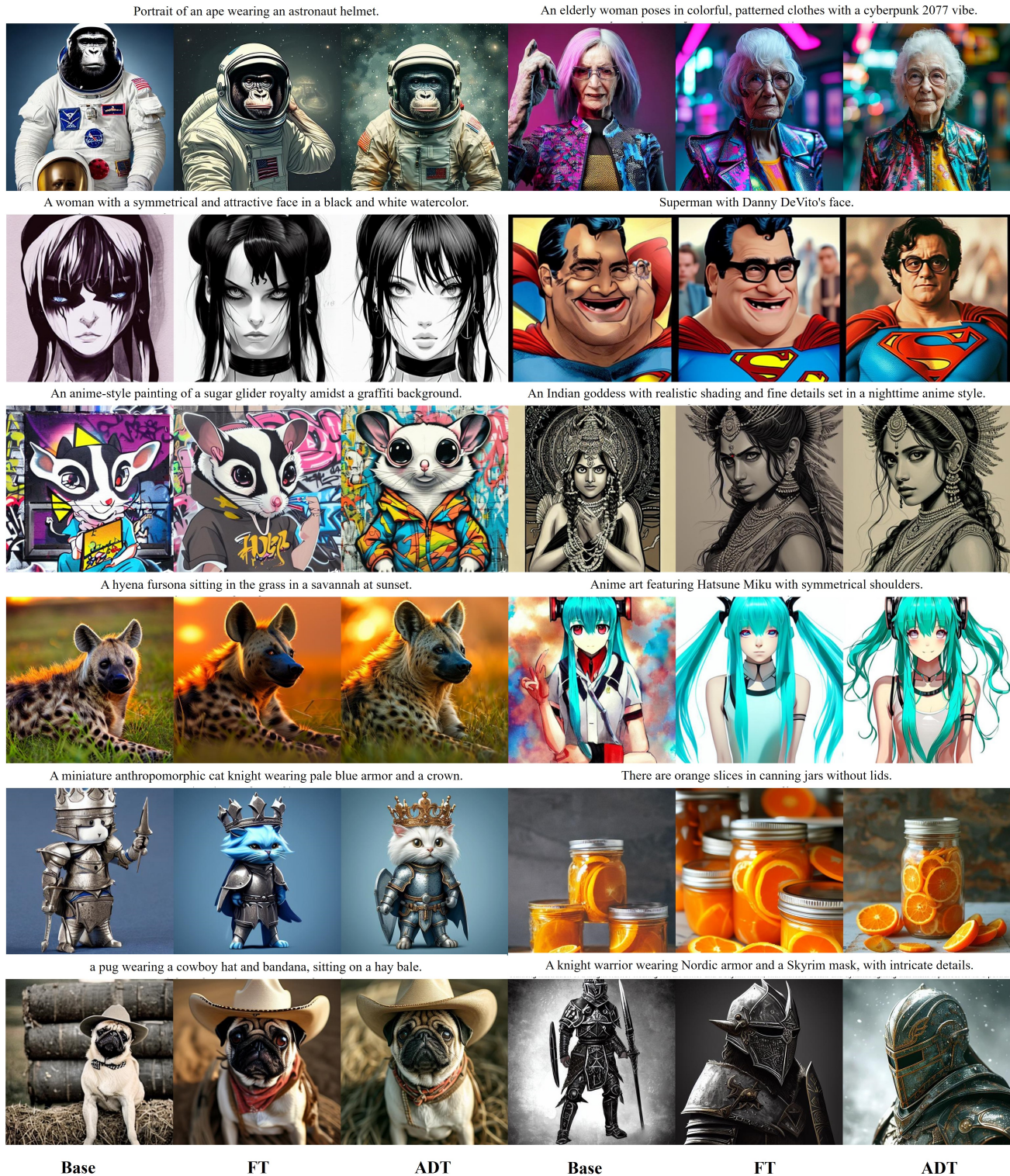


Figure A3. More qualitative results for SD15 with the DDIM sampler and 50 inference steps. Prompts are listed above the picture.

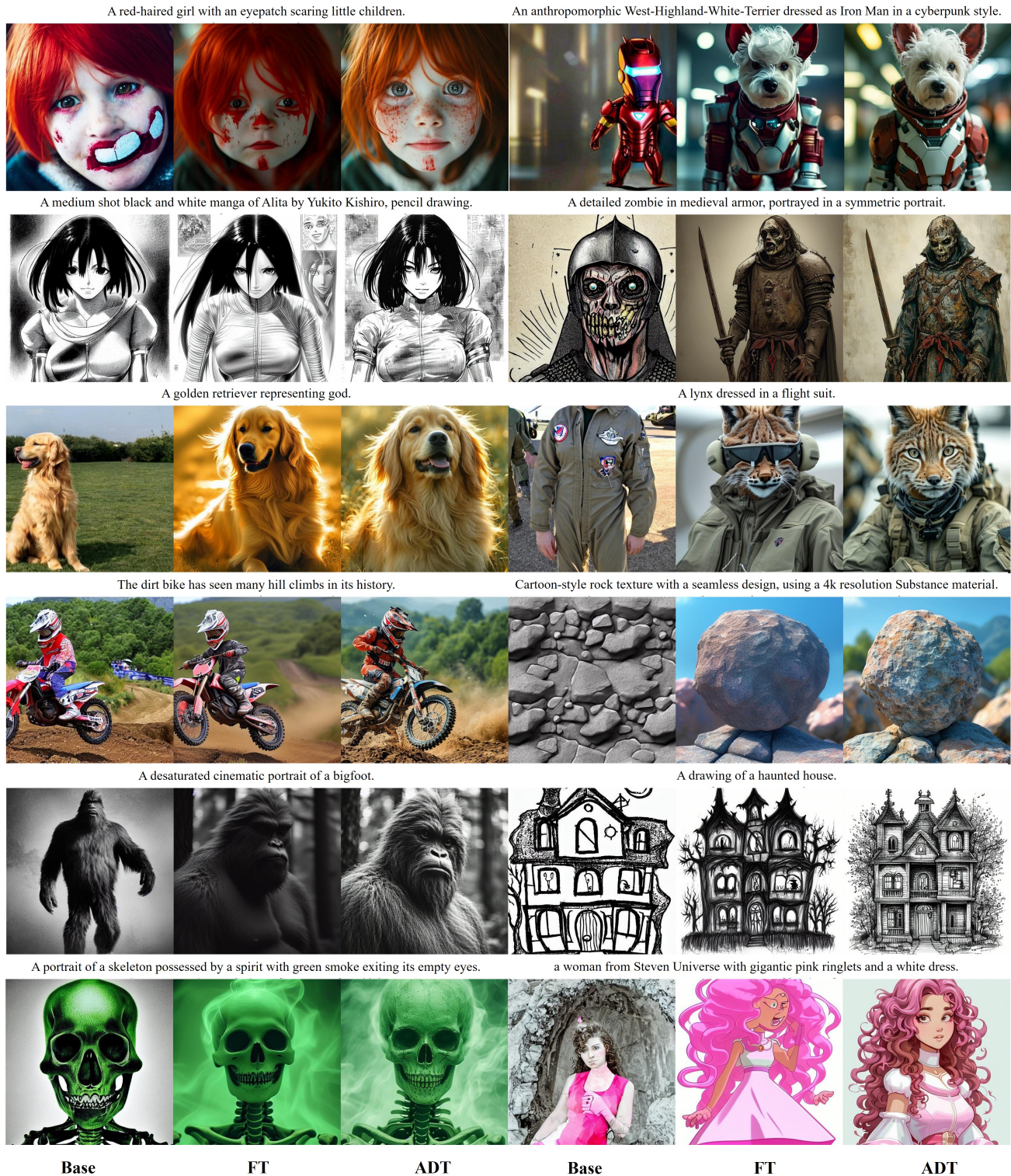


Figure A4. More qualitative results for SD15 with the DPMSlover++ sampler and 30 inference steps. Prompts are listed above the picture.

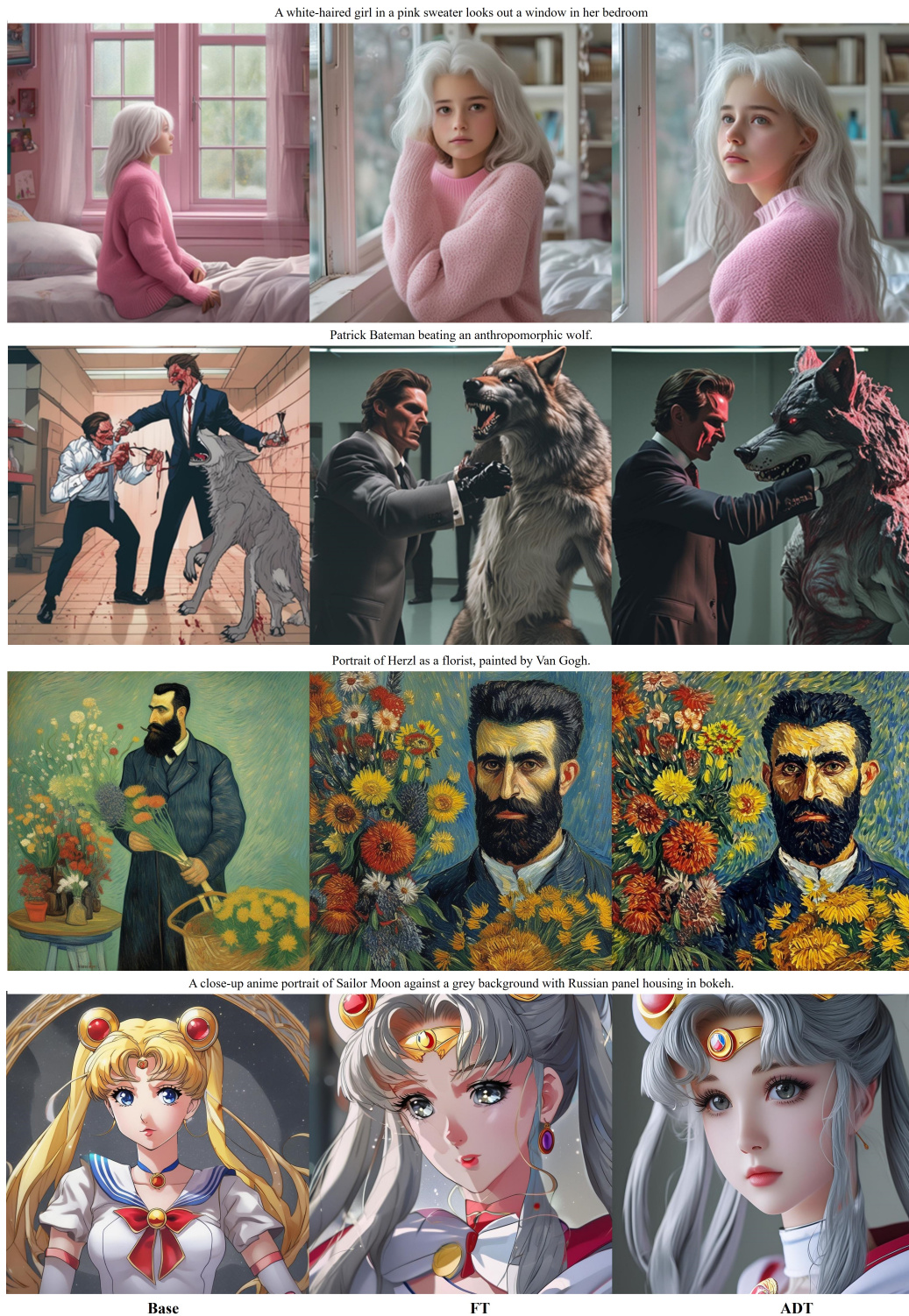


Figure A5. More qualitative results for SDXL with the DDIM sampler and 50 inference steps. Prompts are listed above the picture.

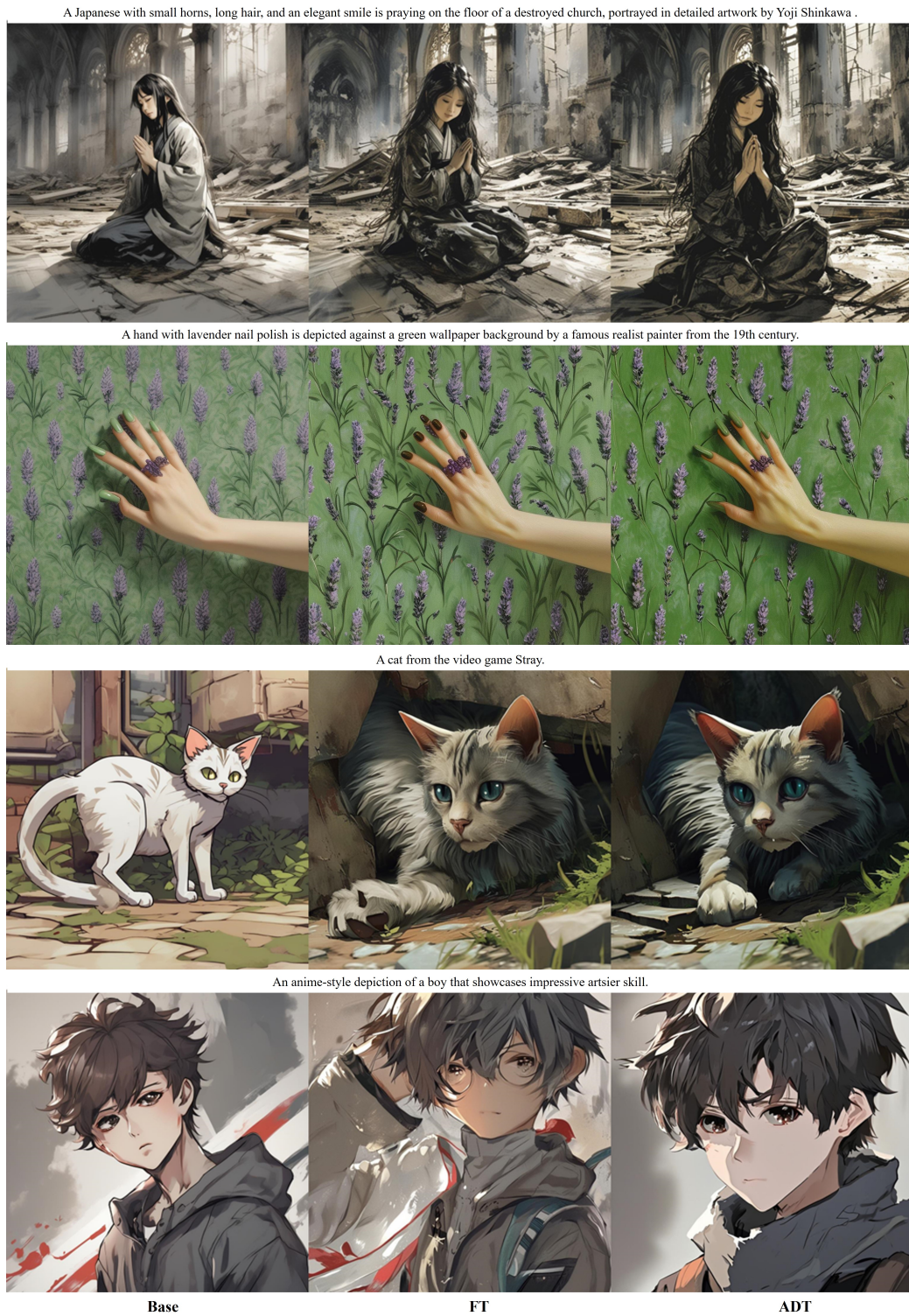


Figure A6. More qualitative results for SDXL with the DDIM sampler and 50 inference steps. Prompts are listed above the picture.



Figure A7. More qualitative results for SDXL with the DPMSlover++ sampler and 30 inference steps. Prompts are listed above the picture.



Figure A8. More qualitative results for SDXL with the DPMSlover++ sampler and 30 inference steps. Prompts are listed above the picture.



Figure A9. More qualitative results for SD3. Prompts are listed above the picture.

A male android, half robot and half humanoid, resembling soccer player Antoine Griezmann, stands still inside a museum exhibit with shiny skin and a blank stare.



Portrait of Archduke Franz Ferdinand by Charlotte Grimm, depicting his detailed face.



Male character illustration by Gaston Bussiere.



Beige canvas tents set up in an arctic landscape with no vegetation, surrounded by rolling hills - reminiscent of a romanticist painting.



Figure A10. More qualitative results for SD3. Prompts are listed above the picture.